ARTICLE

Coherent Spin Transport Through a Six-Coordinate FeN_6 Spin-Crossover Complex with Two Different Spin Configurations

Yue Gu[a], Jing Huang[b*], Yu-jie Hu[a], Qun-xiang Li[a,c*]

a. Department of Chemical Physics, University of Science and Technology of China, Hefei 230026, China
b. School of Materials and Chemical Engineering, Anhui Jianzhu University, Hefei 230601, China
c. Hefei National Laboratory for Physical Sciences at the Microscale, University of Science and Technology of China, Hefei 230026, China

(Dated: Received on May 28, 2019; Accepted on June 2, 2019)

Due to the magnetic bistability, single-molecule spin-crossover (SCO) complexes have been considered to be the most promising building blocks for molecular spintronic devices. Here, we explore the SCO behavior and coherent spin transport properties of a six-coordinate FeN_6 complex with the low-spin (LS) and high-spin (HS) states by performing extensive first-principles calculations combined with non-equilibrium Green's function technique. Theoretical results show that the LS↔HS spin transition via changing the metal-ligand bond lengths can be realized by external stimuli, such as under light radiation in experiments. According to the calculated zero-bias transmission coefficients and density of states as well as the I-V curves under small bias voltages of FeN_6 SCO complex with the LS and HS states sandwiched between two Au electrodes, we find that the examined molecular junction can act as a molecular switch, tuning from the OFF (LS) state to the ON (HS) state. Moreover, the spin-down electrons govern the current of the HS molecular junction, and this observed perfect spin-filtering effect is not sensitive to the detailed anchoring structure. These theoretical findings highlight this examined six-coordinate FeN_6 SCO complex for potential applications in molecular spintronics.

Key words: Transport, Molecular switch, Spin-filtering, Electronic structure, First-principles

I. INTRODUCTION

By using the electron and spin degrees of freedom at the single-molecule level, molecular spintronics has become a rapidly developing field in recent years [1–4], since it holds potential applications in the next generation of electronic devices, especially in quantum computing, and the logical and memory units of computers [5, 6]. Till now, based on different single-molecule magnets or magnetic molecules, various molecular spin devices, such as spin-crossover, spin valve, spin filter, and molecular switch, have been successfully demonstrated or proposed [7–10].

Due to the magnetic bistability, single-molecule spin-crossover (SCO) complexes have been considered as one of the most possible building blocks in molecular spintronics [11, 12]. In general, the spin transition between the low-spin (LS) and high-spin (HS) states can be achieved by external stimuli, such as magnetic or electric field, light, temperature, or strain [13–16]. Among various Fe-based SCO complexes, the mononuclear Fe family, in which the central Fe cation is six-coordinated via N atoms in ligands, has been best studied since their SCO electronic and transport properties are rather easily controlled. Previous research activities mainly focused on SCO behavior, photoswitching, temperature-dependent magnetism [17–21], we should pay more attention to their transport properties of Fe(II)-based SCO complexes.

Very recently, Liu *et al.* have successfully synthesized a new mononuclear Fe(II) SCO complex [22], namely, $[Fe(^{2Me}L_{p_z})(NCX)_2]$ ($^{2Me}L_{p_z}$=*N*, *N*′-dimethyl-*N*, *N*′-bis(2-pyridylmethyl)-1,2-ethanediamine, and X=BH_3), in which the central Fe(II) cation is coordinated by six N atoms in pyrazine-based tetradentate and $NCBH_3$ ligands (for short, named this Fe(II)-based SCO complex as FeN_6 in this work). In their experiments, the complete and abrupt LS↔HS spin transition was realized by temperature and light-induced triggers [22]. This stimulates us to further explore whether this kind of six-coordinated mononuclear Fe(II) complex is a promising building block in molecular spintronic devices.

Based on first-principles calculations combined with

*Authors to whom correspondence should be addressed.
E-mail: jhuang@ustc.edu.cn, liqun@ustc.edu.cn

non-equilibrium Green's function method, we explore the SCO behavior and coherent spin transport properties of FeN_6 complex with two different spin configurations. Theoretical results show that the LS→HS spin transition can be achieved by external stimuli via changing the metal-ligand bond lengths. The current through FeN_6 SCO complex sandwiched between two Au electrodes the molecular junction with the LS state is significantly less than that of the HS state. Moreover, the examined molecular junction with the HS state shows a robust spin-filtering effect, and the current is mainly contributed by the spin-down electrons, which is not sensitive to the anchoring structure.

II. COMPUTATIONAL METHODS

Gaussian package [23] at the meta-GGA hybrid TPSSh functional level, using the triple zeta valence basis set [24], can predict reliable electronic energies and reproduce well the metal-ligand bond lengths of the mononuclear Fe(II) SCO complexes [25–27]. In the work, we adopt the Gaussian Package to optimize the geometric structure, to calculate electronic structure, and to describe SCO behavior of free FeN_6 complex. In our calculations, the convergence criteria for the optimization are set to 10^{-3} atomic unit (a.u.) on the gradient, 10^{-3} a.u. on the displacement, and 10^{-6} a.u. on the energy, respectively.

The coherent transport through the molecular junction is explored by performing density functional theory (DFT) calculations combined with non-equilibrium Green's function (NEGF) technique, implemented in the Atomistix Toolkit (ATK) code [28–30]. The Troullier-Martins pseudopotential is adopted for the calculation for the inner electrons. As for the exchange and correlation functional, we use the generalized gradient approximation in the Perdew-Burke-Ernzerhof form [31]. To balance the calculation precision and costs, double zeta plus polarization basis set is set for all atoms, except for Au atoms, which are described by single zeta plus polarization. We employ $1\times1\times100$ k-points in the Monkhorst Pack, 150 Ry mesh cutoff energy for the real-space grid, and 300 K electron temperature in our calculations.

To obtain spin-resolved current through the molecular junction, the transmission coefficients of the molecular junctions are calculated using

$$T_\sigma(E,V) = \mathrm{Tr}[\Gamma_\mathrm{L} G_\sigma \Gamma_\mathrm{R} G_\sigma^+] \tag{1}$$

where σ stands for the spin-up (↑) and spin-down (↓) channels, $\Gamma_{\mathrm{L/R}}$ is the coupling matrix between the extended molecule and left/right electrode, defined as

$$\Gamma_{\mathrm{L/R}} = \frac{i}{2}\left(\Sigma_{\mathrm{L/R}} - \Sigma_{\mathrm{L/R}}^\dagger\right) \tag{2}$$

and G_σ is the spin-dependent retarded Green's function of the extended molecule, calculated by:

$$G_\sigma = [(E+i\eta)S_\mathrm{C} - H_\mathrm{C} - \Sigma_\mathrm{R} - \Sigma_\mathrm{L}]^{-1} \tag{3}$$

here, H_C and S_C stand for the Hamiltonian and overlap matrices of the extended molecule, η is a small number and $\Sigma_{\mathrm{L/R}}$ is the self-energy due to the presence of the left/right electrode, which is calculated by

$$\Sigma_{\mathrm{L/R}} = V_{\mathrm{L/R}} g^s_{\mathrm{L/R}} V^\dagger_{\mathrm{L/R}} \tag{4}$$

where $g^s_{\mathrm{L/R}}$ is the surface Green's function of the left/right electrode, $V_{\mathrm{L/R}}$ is the interaction between the extended molecule and left/right electrode.

Then, the current through the molecular junction is obtained by

$$I(V) = \frac{e}{h}\int T_\sigma(E,V)[f(E-\mu_\mathrm{L}) - f(E-\mu_\mathrm{R})]\mathrm{d}E \tag{5}$$

where $f(E-\mu)$ is the Fermi-Dirac function for the left and right electrodes with the chemical potential $\mu_{\mathrm{L/R}}$. In this work, we assume that the phase-breaking mean free path is larger than the length of the active transport channel, meaning that the transport of the two spin channels is coherent.

III. RESULTS AND DISCUSSION

Firstly, we optimize the geometric structures of FeN_6 SCO complex with the HS and LS states using the Gaussian Package at the meta-GGA hybrid TPSSh functional level. The initial atomic positions are taken from the crystal structures in a previous experiment [22]. FIG. 1 (a) and (b) illustrate the optimized structures of FeN_6 complex with the LS and HS states, in which three typical Fe−N distances (Fe−N_1, Fe−N_2, and Fe−N_3) are labeled, here, N_1, N_2, and N_3 stand for the N atom in the amine, pyrazine, and $NCBH_3^-$ ligands, respectively. As for the LS state, Fe−N_1, Fe−N_2, and Fe−N_3 is predicted to be about 2.072, 1.966, and 1.923 Å, while they are 2.335, 2.193, and 2.055 Å in the HS configuration, respectively. These predicted Fe−N bond lengths are very close to the experimental values [22]. It is clear that the average Fe−N distance for the HS state is about 2.194 Å, which is longer than that of the LS state by about 0.207 Å. In pseudo-octahedral coordination, the longer Fe−N distance corresponds to the weaker FeN_6 ligand field. Namely, for the HS configuration the d-electron pairing energy is larger than the ligand-field splitting energy, four of six 3d electrons of Fe(II) cation occupy t_{2g} orbital and two 3d electrons occupy $4e_g$ orbital, and then the total spin is S=2. In contrast, for the LS state (S=0), the relatively shorter Fe−N distance results in the relatively strong ligand field, in which the d-electron pairing energy is less than the ligand-field splitting energy, and six 3d electrons show t_{2g}^6 configuration (t_{2g} orbital is 3-fold degenerated). In other words, the LS state is nonmagnetic,

DOI:10.1063/1674-0068/cjcp1905104

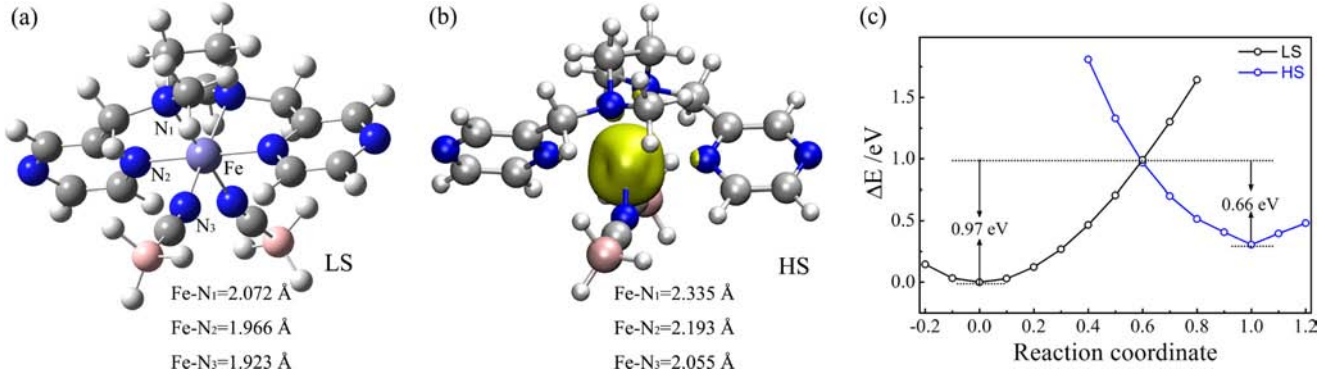

FIG. 1 Optimized structures of free FeN_6 complex with (a) the LS state at the meta-GGA hybrid TPSSh functional level, (b) spin density for the HS state, (c) relative electronic energies of FeN_6 complex with the HS and LS states as a function of the reaction coordinates.

while there are four unpaired 3d electrons in the HS configuration. This is verified by the calculated spin density, localizing around the central region of FeN_6 complex, as shown in FIG. 1(b). The molecular magnetic moment of free HS FeN_6 SCO complex is about 4.0 μ_B (Bohr magneton), which is mainly contributed by the six-coordinate Fe(II) cation.

To describe the spin transition between the LS and HS states at the meta-GGA hybrid TPSSh functional level, we calculate the total electronic energies of free FeN_6 complex with two different spin configurations as a function of the reaction coordinates (X). FIG. 1(c) shows the calculated results, in which X=1 and X=0 label for the energy minimum of the HS and LS states, respectively. In our calculations, X is interpolated between the X=0 (LS) and X=1 (HS) geometry, similar to the previous investigation [32]. Here, X<0 implies that the local Fe−N distance in free FeN_6 with the LS state is shortened, while X>0 labels for the elongated Fe-N distances. As for the HS state, X>1 and X<1 stands for the elongated and shortened Fe−N distances, respectively. As expected, the ground state of FeN_6 complex is LS. The energy difference, defined as $\Delta E = E_{HS} - E_{LS}$, is predicted to be about 310 meV. Since the change of the local Fe−N distances alters the local Fe−N_6 ligand field strength, when X gradually increases to be about 0.6, we observe an LS→HS spin transition, indicating that the local Fe−N_6 ligand field becomes weak due to the relatively long Fe−N distances. Of course, this metal-ligand bond length change inducing spin transition can be easily realized in experiments by applying external stimuli, *i.e.* light irradiation [22].

Now we turn to analyze the frontier orbitals of free FeN_6 complex with two different spin configurations. FIG. 2 illustrates the energy position and the spatial distribution of the HOMO (the highest occupied molecular orbital) and LUMO (the lowest unoccupied molecular orbital). As for the LS case, the HOMO lying at −1.30 eV localizes around the central Fe cation and

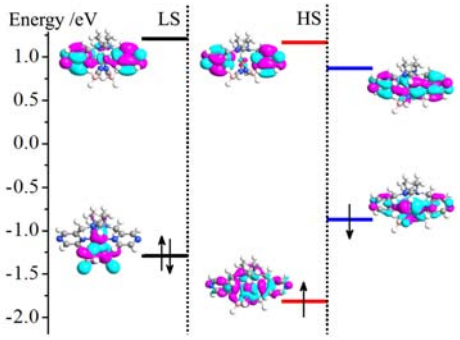

FIG. 2 Energy relative positions and the spatial profiles of the HOMO and LUMO of free FeN_6 SCO complex with two different spin configurations.

two $NCBH_3^-$ ligands, the LUMO locating at 1.20 eV localizes around two pyrazine ligands, and the HOMO-LUMO gap of 2.50 eV is observed. For the spin-up electrons with the HS state, the HOMO at −1.82 eV displays a delocalized feature, the LUMO at 1.21 eV localizes around two pyrazine ligands, while the LUMO and HOMO of the spin-down electrons locating respectively at 0.87 and −0.87 eV are both delocalized on the main body of the complex. The corresponding HOMO-LUMO gaps for the spin-down and spin-up electrons are predicted to be 1.74 and 3.03 eV, respectively. In general, these obvious differences in the geometric and electronic structures of free FeN_6 complex with two different spin configurations will lead to different transport properties.

To explore the coherent transport properties through FeN_6 complex with two different spin configurations, the examined FeN_6 SCO complex is directly connected to the hollow site (the most stable one, compared with the bridge and atop anchoring sites) of left and right Au(111) electrodes modeled by two (6×6) supercells, shown in FIG. 3(a). In addition to left and right Au electrodes, the proposed molecular junction includes

DOI:10.1063/1674-0068/cjcp1905104

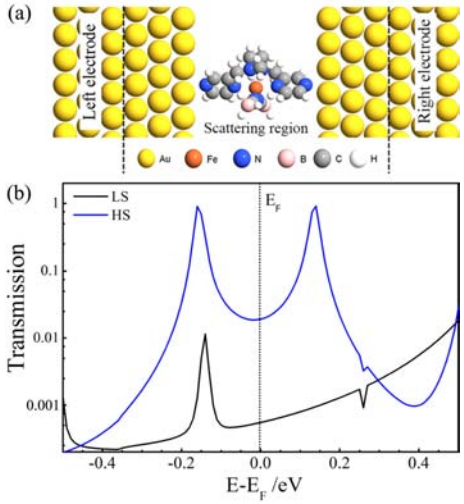

FIG. 3 (a) Schematic model of FeN_6 molecular junction, (b) the zero-bias transmission spectra of FeN_6 molecular junction with the LS (black line) and HS (blue line) states, and the vertical dotted line stands for the Fermi level.

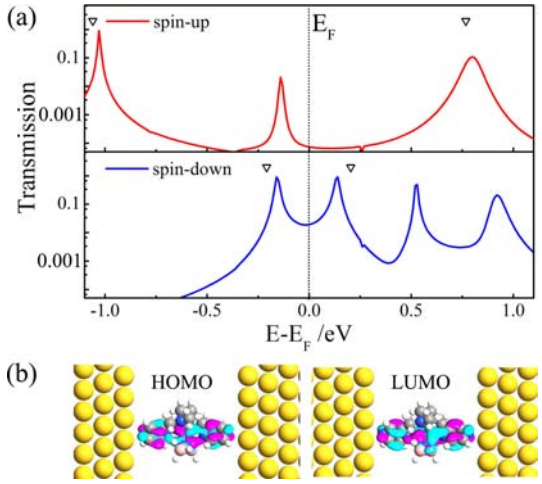

FIG. 4 (a) Zero-bias spin-resolved transmission spectra of FeN_6 molecular junction with the HS state for two spin channels. Here, the top panel for the spin-up electrons, while the bottom panel for the spin-down electrons, the empty triangles denote the positions of the perturbed HOMO and LUMO of the two different spin channels, and the vertical dotted line stands for the Fermi level. (b) Spatial profile of the perturbed HOMO (left) and LUMO (right) of the spin-down channel.

the central scattering region, which contains the sandwiched FeN_6 SCO complex and surface layers of two electrodes. Note that this kind of N-Au connection in molecular devices has been adopted in a previous report [33]. For example, the conductance of a single pyrazine molecular junction reported in the theoretical study is in fair agreement with the experimental results. In our calculations, two N atoms at the two opposite ends of FeN_6 SCO complex are anchored at the stable hollow sites. According to the total energy calculations, we find that the energy preferred N−Au bond length is about 2.3 Å, which is a typical distance in previous investigations [33, 34].

FIG. 3(b) plots the zero-bias transmission spectra of FeN_6 molecular junction with two different spin configurations. Here, the Fermi level is set to zero for clarity. It is clear that the zero-bias transmission spectra of the molecular junctions with the LS and HS states show remarkable different features. As for the LS state, there is only a small and sharp transmission peak located at −0.14 eV, while there are two broad transmission peaks at −0.16 and 0.14 eV. At the Fermi level, the transmission coefficient of FeN_6 molecular jucntion with the LS and HS states is 5.501×10^{-4} and 0.019 G_0 (G_0 denotes the quantum constant and equals to e^2/h). This observation implies that the conductive ability of FeN_6 molecular junction with the LS state under small bias voltages is significantly less than that of the HS state, leading to a molecular switching behavior. That is to say, external stimuli can trigger the LS→HS spin transition, then the FeN_6 molecular junction can be tuned from the OFF state to the ON state.

As for the HS state, free FeN_6 SCO complex has 4.0 μ_B. Therefore, we calculate the zero-bias spin-resolved transmission spectra of the molecular junction with the HS state, and the corresponding results are plotted in FIG. 4(a). Here, empty triangles denote the perturbed HOMO and LUMO of two spin channels. As for the spin-up channel, the transmission coefficients are very small in the relatively large energy window from −0.75 eV to 0.75 eV. While for the spin-down electrons, there are two significant transmission peaks lying at −0.16 and 0.16 eV, which are contributed by the perturbed HOMO and LUMO of the spin-down electrons, as shown in FIG. 4(b). To quantify the transport difference between the spin-up and spin-down channels, we define spin filtering efficiency (SFE) as $|(T_\downarrow-T_\uparrow)/(T_\downarrow+T_\uparrow)|\times100\%$, here, $T_\downarrow$ and $T_\uparrow$ stand for the transmission coefficient of the spin-down and spin-up electrons at the Fermi level. The $T_\uparrow$ and $T_\downarrow$ are calculated to be 0.019 and 7.429×10^{-5}, and then, the SFE is predicted to be 99.2%. Clearly, as for the HS state, the examined FeN_6 molecular junction shows a nearly perfect spin-filtering effect. In other single-molecule magnets or magnetic molecules, such as ligand-driven light-induced spin-change Fe-based SCO complex [35], Fe(II)-N_4S_2 complex [36], Fe_2 SCO complex [37], Fe_4-based complex [38], and Fe-cyclooctatetraene cluster [39], similar spin-filtering effect governed by the spin-down electrons has been observed.

We calculate the total density of states (DOS) of FeN_6 SCO complex with two different spin configurations, and plot them in FIG. 5, since it is helpful to further understand why the conductance of FeN_6 molecular junction with the LS state is less than that of the HS state. The main feature of the DOS curves corresponds

DOI:10.1063/1674-0068/cjcp1905104

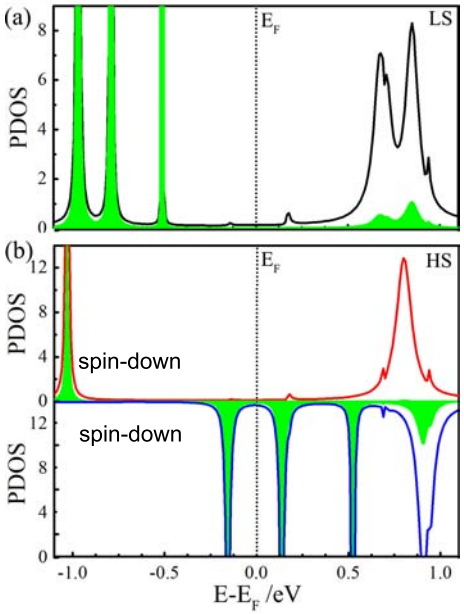

FIG. 5 The total DOS of FeN_6 SCO complex and the PDOS (partial DOS) of the central Fe(II) cation (labeled with the filled green regions), (a) for the LS state and (b) for the HS state, here, the top panels for the spin-up electrons, while the bottom panels for spin-down electrons, and the vertical dotted line stands for the Fermi level.

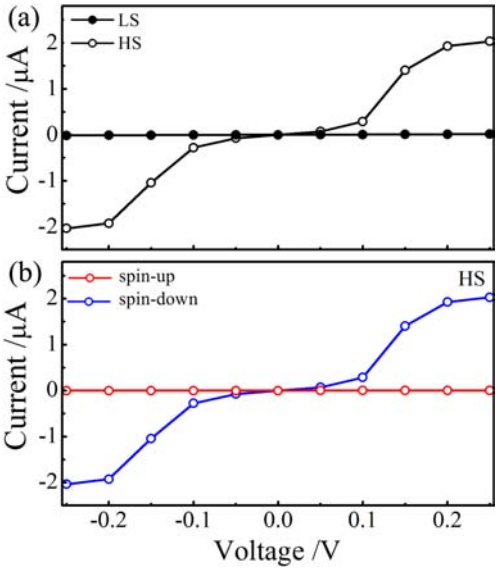

FIG. 6 (a) The I-V curves of FeN_6 molecular junction with the LS and HS states, (b) spin-resolved I-V curves of FeN_6 molecular junction with the HS state. Here, the current of the spin-up electrons are labeled with the red line, while the blue line is for the spin-down electrons.

well with the predicted transmission spectra in FIG. 3(b) and FIG. 4(a). For example, there are four DOS peaks for the HS state lying at −1.03, −0.16, 0.14, and 0.52 eV, which contribute to the transmission peaks at −1.03, −0.16, 0.14, and 0.52 eV, respectively. Clearly, the conductance of the HS state is mainly determined by the tail of the transmission peaks originating from the perturbed HOMO and LUMO. While for the LS state, there is no DOS peaks within the energy window from −0.45 eV to 0.45 eV, resulting in the small transmission coefficients. Therefore, these observations can be used to understand the huge difference of transport properties of two different spin configurations, as shown in FIG. 3(b).

To make sure that the predicted molecular switching and the spin-filtering devices can work under small bias voltages, we calculate the current-voltage (I-V) curves of FeN_6 molecular junction with two different spin states as well as the spin-resolved I-V curves of the HS state under the bias range of [−0.25, 0.25] V, and plot them in FIG. 6 (a) and (b), respectively. In our calculations, based on the Landauer-Büttiker formula, the current is self-consistently calculated at each bias voltage using the non-equilibrium condition. One can see that, the current through FeN_6 molecular junction with the LS state is significantly less than that of the HS configuration. For example, the I_{LS} and I_{HS} are predicted to be 0.01 and 1.93 μA at the applied bias voltage of 0.2 V, respectively. This result implies that FeN_6 molecular junction can act as a molecular switch under small bias voltages.

As for the HS state, the spin-up current ($I_\uparrow$) through FeN_6 molecular junction is significantly less than that of the spin-up electrons ($I_\downarrow$). That is to say, the spin-down electrons give the main contribution to the current through molecular junction with the HS state. To quantify the difference between the spin-up and spin-down currents under different bias voltages, we define the ratio of current of two spin channels as $R(V)=|I_\downarrow(V)/I_\uparrow(V)|$. Within the examined bias window, the $R(V)$ varies in the range of [300, 1500]. For example, at the applied bias voltage of 0.2 V, the R is about 1100. Such a large ratio ensures FeN_6 SCO complex for the real applications, such as acting as a molecular spin filter. Actually, in the bias window of [0.1, 0.2] V, the SFE varies from 99.58% to 99.82% according to the different SFE defined as $|I_\uparrow-I_\downarrow|/|I_\uparrow+I_\downarrow|\times100\%$.

In experiments, it is very difficult to design the exact anchoring structure between the central sandwiched molecule and electrodes, which always alters the transport behavior [40, 41], For example, Parashar *et al.* have shown that the transport properties of molecular junction depended on the adopted electrodes and the anchoring-atom [42]. Here, we finally calculate the zero-bias transmission curves of the HS FeN_6 molecular junction with a different anchoring structure as an example, as shown in FIG. 7(a), in which one Au atom is added on the surface of the left and right electrodes, mimicking tips of scanning probe microscope. The calculated transmission spectra are plotted in FIG. 7(b). It is clear that the transport properties of FeN_6 molec-

DOI:10.1063/1674-0068/cjcp1905104

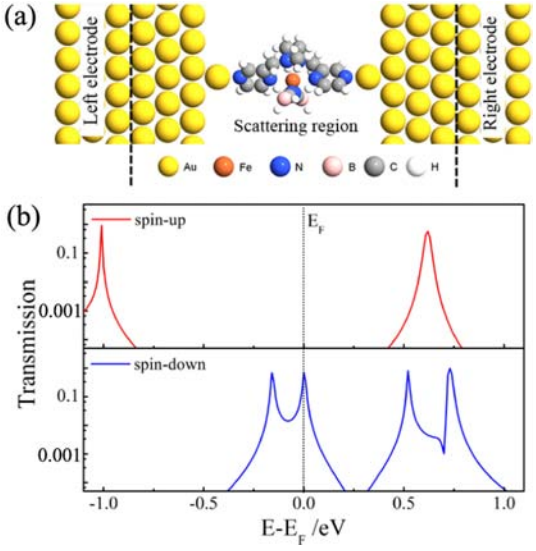

FIG. 7 (a) Schematic model of FeN_6 HS molecular junction with a different anchoring structure. (b) Spin-resolved zero-bias transmission spectra of the spin-up (top panel) and spin-down (bottom panel) electrons. Here, the vertical dotted line stands for the Fermi level.

ular junction are not sensitive to the detailed anchoring structure. The shape and the position of these transmission peaks are similar to the above presented results shown in FIG. 4. The spin-down electrons still govern the conductance. This observation highlights the practical applications of FeN_6 SCO complexes in future molecular spintronics.

IV. CONCLUSION

Based on DFT calculation in combination with NEGF technique, we investigate the SCO behavior and coherent transport properties of a six-coordinate FeN_6 complex with two different spin configurations. The ground state of FeN_6 complex turns out to be the LS state, and the LS→HS spin transition can be triggered by external stimuli via altering the metal-ligand bond lengths. Due to the instinctive differences in the electronic structures, the current through LS FeN_6 molecular junction is significantly less than that of the HS state, resulting in a molecular switching behavior. Moreover, the spin-down electrons govern the current of FeN_6 molecular junction with the HS state, then we observe a nearly perfect spin-filtering effect, which is not sensitive to the detailed anchoring structure. These theoretical findings suggest that the examined six-coordinate FeN_6 complex holds promising for the application in molecular spintronics.

V. ACKNOWLEDGMENTS

This work was partially supported by the National Key Research & Development Program of China (No.2016YFA0200600) and the National Natural Science Foundation of China (No.21873088 and No.11634011). Computational resources are provided by Chinese Academy Sciences, Shanghai and University of Science and Technology Supercomputer Centers.

[1] A. H. Flood, J. F. Stoddart, D. W. Steuerman, and J. R. Heath, Science **306**, 2055 (2004).
[2] M. A. Ratner and A. Aviram, Chem. Phys. Lett. **29**, 277 (1974).
[3] A. S. Martin, J. R. Sambles, and G. J. Ashwell, Phys. Rev. Lett. **70**, 218 (1993).
[4] T. Kim, Z. F. Liu, C. Lee, J. B. Neaton, and L. Venkataraman, Proc. Natl. Acad. Sci. USA **111**, 10928 (2014).
[5] J. M. Clemente-Juan, E. Coronado, and G. Alejandro, Chem. Soc. Rev. **41**, 7464 (2012).
[6] A. P. De Silva and S. Uchiyama, Nat. Nanotech. **2**, 399 (2007).
[7] C. Lefter, V. Davesne, L. Salmon, G. Molnar, P. Demont, A. Rotaru, and A. Bousseksou, Magnetochemistry **2**, 18 (2016).
[8] Z. H. Xiong, D. Wu, Z. V. Vardeny, and J. Shi, Nature **427**, 821 (2004).
[9] M. Urdampilleta, S. Klyatskaya, J. P. Cleuziou, M. Ruben, and W. Wernsdorfer, Nat. Mater. **10**, 502 (2011).
[10] C. Herrmann, G. C. Solomon, and M. A. Venkataraman, J. Am. Chem. Soc. **132**, 3682 (2010).
[11] K. S. Kumar, I. Šalitroš, Z. Boubegtiten-Fezoua, S. Moldovan, P. Hellwig, and M. Ruben, Dalton Trans. **47**, 35 (2018).
[12] K. S. Kumar and M. Ruben, Coord. Chem. Rev. **346**, 176 (2017).
[13] O. Sato, J. Tao, and Y. Z. Zhang, Angew. Chem. Int. Ed. **46**, 2152 (2007).
[14] P. Gütlich, V. Ksenofontov, and A. B. Gaspar, Coord. Chem. Rev. **249**, 1811 (2000).
[15] T. Miyamachi, M. Gruber, V. Davesne, M. Bowen, S. Boukari, L. Joly, F. Scheurer, G. Rogez, T. K. Yamada, P. Ohresser, E. Beaurepaire, and W. Wulfhekel, Nat. Commun. **3**, 938 (2012).
[16] S. Ohnishi and S. Sugano, J. Phys. C **14**, 39 (1981).
[17] R. González-Prieto, B. Fleury, F. Schramm, G. Zoppellaro, R. Chandrasekar, O. Fuhr, S. Lebedkin, M. Kappes, and M. Ruben, Dalton Trans. **40**, 7564 (2011).
[18] J. M. Holland, J. A. McAllister, Z. Lu, C. A. Kilner, M. Thornton-Pett, and M. A. Halcrow, Chem. Commun. 577 (2001).
[19] S. Murata, K. Takahashi, T. Mochida, T. Sakurai, H. Ohta, T. Yamamoto, and Y. Einaga, Dalton Trans. **46**, 5786 (2017).
[20] J. Yuan, M. J. Liu, C. M. Liu, and H. Z. Kou, Dalton Trans. **46**, 16562 (2017).
[21] W. Phonsri, C. G. Davies, G. N. L. Jameson, B. Moubaraki, J. S. Ward, P. E. Kruger, G. Chastanet, and K. S. Murray, Chem. Commun. **53**, 1374 (2017).
[22] X. Liu, J. Zhou, X. Bao, Z. Yan, G. Peng, M. Rouzières, C. Mathonière, J. L. Liu, and R. Clérac, Inorg. Chem. **56**, 12148 (2017).

DOI:10.1063/1674-0068/cjcp1905104

[23] M. J. Frisch, G. W. Trucks, H. B. Schlegel, G. E. Scuseria, M. A. Robb, J. R. Cheeseman, G. Scalmani, V. Barone, B. Mennucci, G. A. Petersson, H. Nakatsuji, M. Caricato, X. Li, H. P. Hratchian, A. F. Izmaylov, J. Bloino, G. Zheng, J. L. Sonnenberg, H. Hada, M. Ehara, K. Toyota, R. Fukuda, J. Hasegawa, M. Ishida, T. Nakajima, Y. Honda, O. Kitao, H. Nakai, T. Vreven, J. A. Montgomery, Jr., J. E. Peralta, F.Ogliaro, M. Bearpark, J. J. Heyd, E. Brothers, K. N. Kudin, V. N. Staroverov, R. Kobayashi, J. Normand, K. Raghavachari, A. Rendell, J. C. Burant, S. S. Iyengar, J. Tomasi, M. Cossi, N. Rega, J. M. Millam, M. Klene, J. E. Knox, J. B. Cross, V. Bakken, C. Adamo, J. Jaramillo, R. Gomperts, R. E. Stratmann, O. Yazyev, A. J. Austin, R. Cammi, C. Pomelli, J. W. Ochterski, R. M. Martain, K. Morokuma, V. G. Zakrzewski, G. A.Voth, P. Salvador, J. J. Dannenberg, S. Dapprich, A. D. Daniels, O. Farkas, J. B. Foresman, J. V. Ortiz, J. Cioslowski, and D. J. Fox, *Gaussian 09, Revision A.1*, Wallingford, CT: Gaussian, Inc., (2009).
[24] A. Schäfer, C. Huber, and R. Ahlrichs, J. Chem. Phys. **100**, 5829 (1994).
[25] J. Cirera and F. Paesani, Inorg. Chem. **51**, 8194 (2012).
[26] K. P. Jensen and J. Cirera, J. Phys. Chem. A **113**, 10033 (2009).
[27] G. S. Matouzenko, S. A. Borshch, V. Schünemann, and J. A. Wolny, Phys. Chem. Chem. Phys. **15**, 7411 (2013).
[28] M. Brandbyge, J. L. Mozos, P. Ordejón, J. Taylor, and K. Stokbro, Phys. Rev. B **65**, 165401 (2002).
[29] J. Taylor, H. Guo, and J. Wang, Phys. Rev. B **63**, 245407 (2001).
[30] M. Büttiker, Y. Imry, R. Landauer, and S. Pinhas, Phys. Rev. B **31**, 6207 (1985).
[31] J. P. Perdew, K. Burke, and M. Ernzerhof, Phys. Rev. Lett. **77**, 3865 (1996).
[32] N. Baadji and S. Sanvito, Phys. Rev. Lett. **108**, 217201 (2012).
[33] X. J. Wu, Q. X. Li, J. Huang, and J. L. Yang, J. Chem. Phys. **123**, 184712 (2005).
[34] S. M. Hou, J. Zhang, R. Li, J. Ning, R. Han, Z. Shen, X. Zhao, Z. Xue, and Q. Wu, Nanotechnology **16**, 239 (2005).
[35] F. F. Li, J. Huang, Y. J. Hu, and Q. X. Li, RSC Adv. **9**, 12339 (2019).
[36] M. L. Du, Y. J. Hu, J. Huang, and Q. X. Li, Chin. J. Chem. Phys. **31**, 33 (2018).
[37] J. Huang, R. Xie, W. Y. Wang, Q. X. Li, and J. L. Yang, Nanoscale **8**, 609 (2016).
[38] F. Zu, Z. Liu, K. Yao, G. Gao, H. Fu, S. Zhu, Y. Ni, and L. Peng, Sci. Rep. **4**, 4838 (2014).
[39] J. Huang, Q. X. Li, K. Xu, H. B. Su, and J. L. Yang, J. Phys. Chem. C **114**, 11946 (2010).
[40] S. Caliskan and A. Laref, Phys. Chem. Chem. Phys. **16**, 13191 (2014).
[41] Z. Li, M. Smeu, M. A. Ratner, and E. Borguet, J. Phys. Chem. C **117**, 14890 (2013).
[42] S. Parashar, Mater. Res. Exp. **5**, 055011 (2018).

DOI:10.1063/1674-0068/cjcp1905104